Inorganic Chemistry

ARTICLE

pubs.acs.org/IC

Synthesis, Structure, Negative Thermal Expansion, and Photocatalytic Property of Mo Doped ZrV_2O_7

Prangya Parimita Sahoo, S. Sumithra, Giridhar Madras, and T. N. Guru Row*

Solid State and Structural Chemistry Unit, Indian Institute of Science, Bangalore 560012, India

Supporting Information

ABSTRACT: A new series of compounds identified in the phase diagram of $ZrO_2-V_2O_5-MoO_3$ have been synthesized via the solution combustion method. Single crystals of one of the compounds in the series, $ZrV_{1.50}Mo_{0.50}O_{7.25}$, were grown by the melt-cool technique from the starting materials with double the MoO_3 quantity. The room temperature average crystal structure of the grown crystals was solved using the single crystal X-ray diffraction technique. The crystals belong to the cubic crystal system, space group $Pa\bar{3}$ (No. 205) with a = 8.8969 (4) Å, V = 704.24 (6) Å^3, and Z = 4. The final R_1 value of 0.0213 was achieved for 288 independent reflections during the structure refinement. The Zr^{4+} occupies the special position (4*a*) whereas V^{5+} and Mo^{6+} occupy two unique (8*c*) Wyckoff positions. Two fully occupied O atoms, (24*d*) and (4*b*), one partially occupied O atom (8*c*) have been identified for this molybdovanadate, which is a unique feature for these crystals. The structure is related to both ZrV_2O_7 and cubic $ZrMo_2O_8$. The temperature dependent single crystal studies show negative thermal expansion above 370 K. The compounds have been characterized by powder X-ray diffraction, solid-state UV−vis diffuse reflectance spectra, scanning electron microscopy (SEM), and transmission electron microscopy (TEM). The photocatalytic activity of these compounds has been investigated for the degradation of various dyes, and these compounds show specificity toward the degradation of non-azoic dyes.

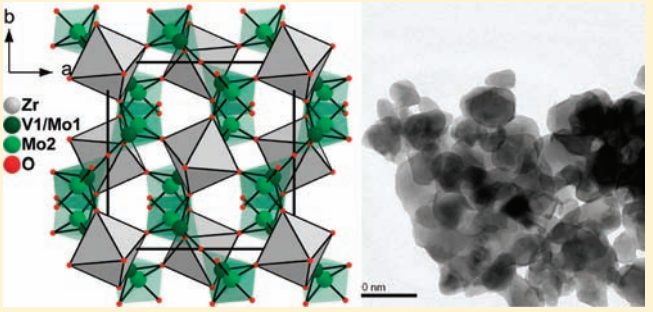

INTRODUCTION

The existence of zirconium pyrovanadate (ZrV_2O_7) was first reported by Peyronel[1] in 1942. It belongs to the AX_2O_7 (A = Zr, Hf and X = P, As, V) families of compounds and has a framework structure with space group symmetry $Pa\bar{3}$, Z = 4. The structure is related to the NaCl structural type (Space group $Fm\bar{3}m$) with A^{4+} cation and $(X_2O_7)^-$ anion. It displays two first order structural phase transitions[2,3] at 77 and 102 °C. ZrV_2O_7 belongs to a 3 × 3 × 3 superstructure at room temperature which vanishes above 102 °C, and a strong isotropic negative thermal expansion behavior is reported for the temperature up to 800 °C. The superstructure for this compound was established from single crystal synchrotron data, high-resolution neutron powder diffraction data, and electron diffraction studies.[4−6] Upon application of pressure, ZrV_2O_7 undergoes a reversible phase transition at 1.38−1.58 GPa from cubic (α phase) to pseudotetragonal (β phase), which displays an orthorhombic 2 × 3 × 3 super cell.[7] The room temperature Raman and infrared spectra of ZrV_2O_7 have been collected at 12 and 5.7 GPa and support the phase transition behavior established by high pressure X-ray diffraction (XRD).[8] Electrical conductivity has also been investigated for ZrV_2O_7 and hot pressed samples show electrical conductivity suggesting semiconductor n-type behavior, which ranges from 10^{-5} to 10^{-6} Ω^{-1} cm^{-1} with an activation energy of 0.2 eV believed to be due to V^{4+} defects.[9] Zirconium vanadate has been successfully utilized as inorganic ion exchanger for the separation of ^{134}Cs and ^{152}Eu from a synthetic mixture.[10] Many solid solutions have been established in this thermal expansion material. A continuous solid solution was isolated in the $ZrV_2O_7-ZrP_2O_7$ ($0 \le x \le 2.0$) series, and the isotropic thermal behavior was studied.[3] A solid solution $Zr_{1-x}Hf_xV_2O_7$ (x = 0−1) has been isolated, and the thermal expansion behavior has been studied.[11] However, aliovalent substitution at the V site has not been reported in the literature. As molybdovanadates have been studied extensively owing to their unique structures[12,13] and interesting properties like catalysis,[14] the effect of substitution of Mo at V site in ZrV_2O_7 has been described in this study. From the available literature, the difficulties associated with the formation of ZrV_2O_7[2,9] are obvious. The reaction between ZrO_2 and V_2O_5 has been described as "extraordinarily slow". To overcome these difficulties, "combustion synthesis", which is a soft-chemical method resulting in the formation of homogenized high purity products with reduced particle sizes and larger surface area,[15,16] has been employed to synthesize the various members of the solid solution, $ZrV_{2-x}Mo_xO_{7+\delta}$ ($0 \le x \le 0.8$, $\delta = x/2$ throughout the article). As negative thermal expansion is an important phenomenon in designing materials with a specific thermal expansion coefficient and achieving zero expansion for

Received: March 18, 2011
Published: August 16, 2011

exact positioning of various devices, we have studied the thermal expansion behavior of the Mo substituted ZrV_2O_7.

The release of dyes from the textile industries contributes substantially toward the environmental contamination.[17] Degradation of the dyes to less harmful byproducts is an effective method for removal of these organic pollutants. Semiconductor photocatalysis provides a great potential for elimination of these toxic chemicals. Though TiO_2 based photocatalysts[18] have been routinely used, recently non-TiO_2 photocatalysts[19] have been receiving a lot of attention. $V_2O_5-ZrO_2$ mixed oxide catalysts have been subjected to various applications like the oxidation of *o*-xylene to phthalic anhydride, oxidative dehydrogenation of propane, and selective oxidation of toluene to benzaldehyde.[20−23] Therefore, a variety of dyes, which are known to be major wastewater pollutants, were degraded utilizing the various members of the solid solution as catalysts.

In this article, we report the characterization of the solid solution by solid state UV−vis diffuse reflectance spectra, Scanning Electron Microscopy (SEM), and Transmission Electron Microscopy (TEM). Single crystals of these Mo doped compounds have been grown by the melt-cool technique to understand the crystallographic modifications by Mo substitution in ZrV_2O_7. Further, in continuation of our research on studying the catalytic properties of the very well studied thermal expansion materials[24,25] like $ZrMo_2O_8$, we have isolated a solid solution $ZrV_{2-x}Mo_xO_{7+\delta}$ ($0 \le x \le 0.8$) in the phase diagram of $ZrO_2-V_2O_5-MoO_3$ and studied the catalytic activity.

EXPERIMENTAL SECTION

Materials. $ZrO(NO_3)_2 \cdot 2H_2O$ (BDH England, 99.99%), NH_4VO_3, $(NH_4)_6Mo_7O_{24} \cdot 4H_2O$, glycine, Methylene Blue (MB), Orange G (OG), Remazol Brilliant Blue R (RBBR), Rhodamine B (RB), Methyl Orange (MO), Acid Orange 6 (AO6), and Acid Orange 7 (AO7) (all from S. D. Fine-Chem Ltd., India, 99%) were used as such. Water was double distilled and filtered through a Millipore membrane filter prior to use.

Synthesis and Single Crystal Growth. All the members of the solid solution $ZrV_{2-x}Mo_xO_{7+\delta}$ ($0 \le x \le 0.8$) were synthesized by the solution combustion method. For the combustion synthesis of the various members of the solid solution, $ZrO(NO_3)_2 \cdot 2H_2O$, $(NH_4)_6Mo_7O_{24} \cdot 4H_2O$, NH_4VO_3 were taken as the precursors, which were dissolved in double distilled water to prepare a clear solution. In case of NH_4VO_3, the solution was warmed to obtain a transparent solution. The stoichiometric ratio of oxidizer to fuel was maintained at unity to achieve the highest exothermicity of the reaction.[26] They were added in a Petri dish and stirred with a magnetic stirrer. The fuel, glycine, was added to the reaction mixture, and the resultant mixture was fired in a preheated furnace maintained at 550 °C for 10 min. When glycine undergoes combustion with precursors, it produces heat that is absorbed by the precursors accelerating the chemical reaction of the precursors. The colors of the products obtained were yellowish to greenish brown.

To obtain better insights into the structural changes, single crystals of the Mo doped ZrV_2O_7 were obtained from the melt-cool technique. ZrO_2, V_2O_5, and MoO_3 were taken in the ratios of 2:1:2. The compounds were ground well, and the resultant mixture was placed in a platinum crucible for heat treatment. Excess MoO_3 was taken, to account for the MoO_3 loss, as it sublimes at temperatures used in the synthesis. Single crystals were obtained by treating the powdered mass at 850 °C for 3 h followed by slow cooling at 5 °C/h down to 800 °C followed by furnace cooling to room temperature. Brown crystals were obtained on the surface of the melt. However, because of the volatile nature of MoO_3, the exact composition of the single crystal is not accessible unless uniquely established by single crystal structure analysis.

Table 1. Single Crystal X- ray Diffraction Data of $ZrV_{1.50}Mo_{0.50}O_{7.25}$

empirical formula	$ZrV_{1.50}Mo_{0.50}O_{7.25}$
formula weight	332.0
crystal habit, color	block, brown-yellow
crystal size/mm	0.30 × 0.20 × 0.05
temperature/K	298(2)
radiation	Mo Kα
wavelength/Å	0.71073
crystal system	cubic
space group	$Pa\bar{3}$
a/Å	8.8969(4)
volume/Å^3	704.24(6)
Z	4
density/g cm^{-3}	3.131
$F(000)$	644
scan mode	ω scan
θ_{max} (deg)	28.31
$h_{min,max}$, $k_{min,max}$, $l_{min,max}$	(−11,4), (−8,11), (−9,10)
no. of reflns. measured	1420
no. of unique reflns.	288
absorption correction	multiscan
μ (mm^{-1})	4.263
no. of parameters	23
refinement	F^2
R_all, R_obs	0.0362, 0.0213
wR_2_all, wR_2_obs	0.0457, 0.0436
Max/min $\Delta\rho$ e/Å^3	0.287, −0.324

Powder XRD. Powder XRD data were collected using a Philips X-pert diffractometer with Cu Kα radiation over the angular range $10° \le 2\theta \le 80°$, with a step width of 0.0167° at room temperature calibrated against Silicon Powder (NIST-SRM 640c) standards. Le Bail profile analysis[27] in the JANA2000 suite was used to refine the XRD data. The background was estimated by a Legendre polynomial function consisting of 15 coefficients, and the peak shapes were described by a pseudo-Voigt function varying five profile coefficients. A scale factor, a zero error factor, and shape were refined.

Single Crystal XRD. A block shaped single crystal (Supporting Information, Figure S1) was selected on the basis of size and sharpness of diffraction spots. Data collection was carried out on an Oxford CCD Diffractometer with Mova MoKα microsource radiation ($\lambda_{Mo\ K\alpha}$ = 0.71073 Å, graphite monochromatized) Eos detector with X-ray generator operating at 49.30 kV and 0.98 mA. The diffraction intensities were corrected for Lorentz and polarization effects. The cell refinement and the data reduction were done using CrysAlis RED[28] (special programs available with the diffractometer). Variable temperature studies from 100 to 480 K were performed with Oxford instruments Cryojet system with a rate of 4 K/h. The room temperature average structure was solved by Patterson Methods using SHELXS97 and refined using SHELXL97 included in the package WinGX, from 288 independent reflections, having $I \ge 2\sigma(I)$.[29,30] The packing diagrams were generated by DIAMOND version 3.2e.[31] Crystallographic data and the details of the single crystal data collection are given in Table 1. Atomic coordinates and isotropic displacement parameters are presented in Table 2. Anisotropic Displacement Parameters (ADPs) and selected interatomic distances are given in Tables 3 and 4. Single-crystal XRD data at 200 and 400 K are also given in the Supporting Information

dx.doi.org/10.1021/ic201224g |*Inorg. Chem.* 2011, 50, 8774–8781

(CIF), for comparison. The crystal data have been deposited at the Fachinformationszentrum Karlsruhe (FIZ) with the CSD number 422130.

Characterization. The analysis of the morphology was performed with the help of a FEI Sirion scanning electron microscope (SEM). Transmission electron microscope (TEM) images were taken from JEOL 2000 FX 11 transmission microscope. UV−vis diffuse reflectance spectra were recorded on a Perkin-Elmer Lambda 35 UV−vis Spectrophotometer.

Photocatalytic Experiments. *Photochemical Reactor.* The photochemical reactor used in this study consists of two parts. The inner part was a jacketed quartz tube of 3.4 cm inner diameter, 4 cm outer diameter, and 21 cm length, while the outer part is a pyrex glass reactor of 5.7 cm inner diameter and 16 cm of length. A high pressure mercury vapor lamp (HPML) of 125 W (Philips, India) was placed inside the jacketed quartz tube after the removal of the outer shell. The fluctuations in the input supply were controlled by a ballast and capacitor, connected in series with the lamp. Water, circulating through the annulus of the quartz tube, maintained the solution at ambient temperature. A 100 mL portion of the solution was taken into the outer reactor and continuously stirred to ensure that the suspension of the catalyst was uniform. The lamp radiated predominantly at 365 nm corresponding to the energy of 3.4 eV, and photon flux was 5.8×10^{-6} mol of photons/s. Further details of the experimental setup can be found elsewhere.[14]

Degradation Experiments. The photocatalytic degradation of seven commonly used dyes covering a wide range of the visible spectrum and diverse functional groups has been investigated. The structures of the dyes are shown in Supporting Information, Table S1. The initial concentrations of the dye solutions varied between 20 to 100 ppm depending on the molar absorptivity (ε) of each dye. The samples were loaded at 1 g/L, and the volume of the dye solution taken was 100 mL in all the experiments. The samples were filtered through Millipore membrane filters and centrifuged to remove the catalyst particles prior to UV analysis.

Sample Analysis. All samples were analyzed with a UV−vis spectrophotometer (Lambda 35, Perkin-Elmer) to quantify the degradation reactions. The calibration for MB, OG, RBBR, RB, MO, AO6, and AO7 were based on the Beer−Lambert law, at their maximum absorption wavelengths, λ_{max} of 664, 489, 591, 554, 464, 490, and 485 nm, respectively. Analysis of the samples using a UV−vis spectrophotometer showed a continuous decrease in the UV−vis absorption at λ_{max} of the starting material, and no new peaks were observed.

Table 2. Atomic Coordinates and Isotropic Displacement Parameters (Å^2) for $ZrV_{1.50}Mo_{0.50}O_{7.25}$, ZrV_2O_7 and High Temperature Form of ZrW_2O_8

	$ZrV_{1.50}Mo_{0.50}O_{7.25}$	ZrV_2O_7[5]	ZrW_2O_8(HT)[35]
atom	**Zr(4*a*)**	**Zr(4*a*)**	**Zr(4*a*)**
x	0	0	0
U_{eq} (Å^2)	0.02106(19)	0.0237(7)	0.014
occupancy	1	1	1
atom	**V1/Mo1 (8*c*)**	**V (8*c*)**	**W1 (8*c*)**
x	0.38772(7)	0.3817(4)	0.3394(5)
U_{eq} (Å^2)	0.0165(2)	0.0156(1)	0.011
occupancy	**0.85(0.75/0.10)**	**1**	**0.5**
atom	**Mo2(8*c*)**		**W2 (8*c*)**
x	0.3364(2)		0.6035(5)
U_{eq} (Å^2)	0.0212(6)		0.011
occupancy	**0.15**		**0.5**
atom	**O1(4*b*)**	**O1(4*b*)**	**O3(8*c*)**
x	1/2	1/2	0.5055
U_{eq} (Å^2)	0.069(2)	0.0811(2)	0.044
occupancy	**1**	**1**	**0.5**
atom	**O1A(8c)**		**O4(8*c*)**
x	0.2267(18)		0.2322(4)
U_{eq} (Å^2)	0.052(10)		0.064
occupancy	**0.14**		**0.5**
atom[a]	**O2(24*d*)**	**O2(24*d*)**	**O1(24*d*)**
x	0.4387(3)	0.4363(4)	0.0549(4)
y	0.2062(2)	0.2058(2)	−0.2089(2)
z	0.4145(3)	0.4070(3)	−0.0671(3)
U_{eq} (Å^2)	0.0485(6)	0.0764(2)	0.036
occupancy	**1**	**1**	**1**

[a] For all other atoms, $x = y = z$.

RESULTS AND DISCUSSION

Crystal Structure. Room temperature single crystal diffraction data were collected on the as grown single crystals, indexed in the cubic crystal system, with $a = 8.8969\ (4)$ Å, $V = 704.24\ (6)$ Å^3, and $Z = 4$. Space group $Pa\bar{3}$ was assigned based on the systematic absences. The positions of the heavy atoms were obtained by direct methods. Zr was located at the 4*a* ($\bar{3}$ axis) Wyckoff site. V atom occupied 8*c* (3-fold axis) Wyckoff site. At this point of the refinement, difference Fourier synthesis revealed significant electron density at another 8*c* (3-fold axis) position. The Mo position was assigned to this site. It is noteworthy that in the crystal structure of ZrV_2O_7 and other substituted compounds there has been only one position identified for V and the

Table 4. Selected Bond Lengths of $ZrV_{1.50}Mo_{0.50}O_{7.25}$

bond length type		distance (Å)
V1/Mo1	-O1	1.7302(10)
	-O2 × 3	1.694(2)
Mo2	-O1A	1.69(3)
	-O2 × 3	1.629(2)
Zr	-O2 × 6	2.059(2)

Table 3. Anisotropic Displacement Parameters (Å^2) of $ZrV_{1.50}Mo_{0.50}O_{7.25}$

atom	U_{11}	U_{22}	U_{33}	U_{12}	U_{13}	U_{23}
Zr(4a)	0.0211(2)	U_{11}	U_{11}	0.0016(2)	U_{12}	U_{12}
V1/Mo1 (8c)	0.0165(2)	U_{11}	U_{11}	0.0018(2)	U_{12}	U_{12}
Mo2(8c)	0.0212(6)	U_{11}	U_{11}	0.0040(8)	U_{12}	U_{12}
O1(4b)	0.069(2)	U_{11}	U_{11}	−0.0211(2)	U_{12}	U_{12}
O1A(8c)	0.0544(14)	U_{11}	U_{11}	−0.022(9)	U_{12}	U_{12}
O2(24d)	0.052(10)	0.0321(13)	0.0590(16)	0.0135(12)	0.0048(14)	0.0109(12)

dx.doi.org/10.1021/ic201224g |*Inorg. Chem.* 2011, 50, 8774–8781

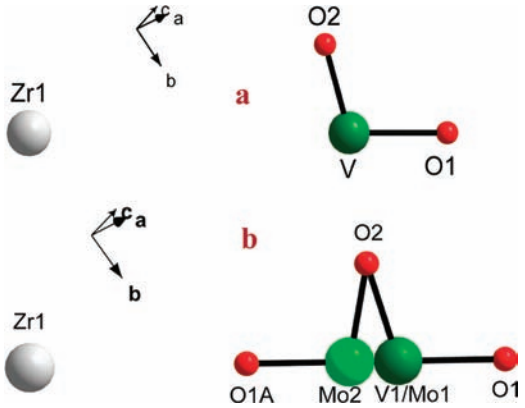

Figure 1. Asymmetric unit view of (a) ZrV_2O_7 and (b) $ZrV_{1.50}Mo_{0.50}O_{7.25}$.

substituted surrogate atom. The total occupancy, of both the sites, was constrained to 1, and the individual ratios were allowed to vary using the PART command in the SHELX package. The two oxygen atom positions were identified by subsequent difference Fourier analysis. Like in case of the parent compound, one oxygen atom (O1) was identified to occupy the 4*b* ($\bar{3}$ axis) site, the other oxygen atom (O2) occupied the 24*d* general position. Both the oxygen atoms were fully occupied. At this stage of refinement, the V:Mo occupancy was fixed at 85:15 derived from the PART command. To account for the Mo incorporation into the crystal structure, Mo1 was introduced in V1. The isotropic displacement parameters and coordinates of Mo1 were fixed as that of V1. The occupancies of V1 and Mo1 were allowed to refine within 85% occupancy restriction, as assigned previously for the V atom. The refined occupancies were fixed afterward. Anisotropic refinements were performed on the Zr, V, and Mo atoms. At this stage of refinement, the highest residual electron density peak (1.09 e/Å^3) at the Wyckoff position 8*c* (3-fold axis) was assigned to be that of an oxygen atom. Indeed, this position is suitable for the Mo−O bond formation. The electron density has been properly modeled when the additional O1A atom is included in the refinement protocol. Partial occupancy was assigned to the O1A atom to charge balance the system. It is to be noted that because of the aliovalent substitution of Mo^{6+} for V^{5+} in ZrV_2O_7, the overall charge is balanced by additional amount of oxygen resulting in $ZrV_{2-x}Mo_xO_{7+\delta}$. For example, in $Fe_2V_{3.16}Mo_{0.84}O_{13.42}$, both V and Mo retain their highest oxidation states, and the charge is balanced by introduced oxygen atoms.[32] The final residual factors are $R_{\_obs}$ = 0.0213 and wR_{2_obs}= 0.0446. The formula derived from single crystal XRD analysis is $ZrV_{1.50}Mo_{0.50}O_{7.25}$.

A comparison of the asymmetric unit of ZrV_2O_7 with that of the Mo substituted $ZrV_{2-x}Mo_xO_{7+\delta}$ is shown in Figure 1. The presence of unique positions for V and Mo is evident from the figure. An additional O atom position (O1A) accounting for the excess amount of oxygen in $ZrV_{2-x}Mo_xO_{7+\delta}$ as compared to the parent compound is also shown in Figure 1. It is of interest to compare the $ZrV_{2-x}Mo_xO_{7+\delta}$, now stoichiometrically fixed as $ZrV_{1.50}Mo_{0.50}O_{7.25}$, with the most widely studied iso-structural negative thermal expansion materials, cubic ZrW_2O_8[33] and $ZrMo_2O_8$.[34] The cubic ZrW_2O_8 and $ZrMo_2O_8$ crystallize in the noncentrosymmetric space group $P2_13$ (No. 198) whereas ZrV_2O_7 crystallizes in the centrosymmetric space group $Pa\bar{3}$ (No. 205). Cubic polymorphs of ZrW_2O_8 (and $ZrMo_2O_8$) and ZrV_2O_7 consist of AO_8 octahedra and XO_4 tetrahedra. However,

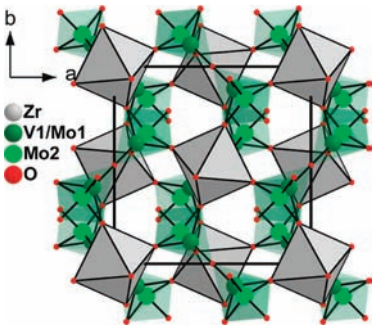

Figure 2. Polyhedral representation of $ZrV_{1.50}Mo_{0.50}O_{7.25}$.

Table 5. Variation of Cell Parameter with Temperature of the Single Crystal

temperature (K)	cell parameter *a* (Å)
100	8.8829(2)
200	8.8895(3)
250	8.8911(2)
270	8.8921(2)
298	8.8969(4)
330	8.9000(2)
360	8.9065(2)
370	8.9075(2)
380	8.9027(3)
400	8.9004(5)
480	8.8965(3)

in ZrV_2O_7, because of the presence of the "bridging" O atom, the tetrahedra form a pyrovanadate group, and a center of inversion is introduced in the system unlike that in cubic ZrW_2O_8.[35] As cubic ZrW_2O_8 is isostructural to cubic $ZrMo_2O_8$ and thermodynamically more stable and well studied in the literature, than the latter, we will compare the Mo doped ZrV_2O_7 with it. ZrW_2O_8 undergoes a phase transformation from the space group $P2_13$ to $Pa\bar{3}$ at 483 K. In this phase, one Zr atom, two unique W atoms and three distinct O atom positions have been identified.[35] Table 2 provides the coordinates of ZrV_2O_7,[5] the current compound of interest, $ZrV_{1.50}Mo_{0.50}O_{7.25}$, and high temperature form of ZrW_2O_8 (HT ZrW_2O_8). It is clear that the structure of $ZrV_{1.50}Mo_{0.50}O_{7.25}$ is a hybrid of ZrV_2O_7 and HT ZrW_2O_8. On careful examination, it is found that the Wyckoff positions for Zr (4*a*), W1 (8*c*), and W2(8*c*) in HT ZrW_2O_8 are the same for Zr, V1/Mo1 and Mo2, respectively in $ZrV_{1.50}Mo_{0.50}O_{7.25}$. One fully occupied O atom (24*d*) and two partially occupied O atoms (8*c* Wyckoff positions each with 0.5 occupancy) are present in HT ZrW_2O_8. Likewise, in $ZrV_{1.50}Mo_{0.50}O_{7.25}$, two fully occupied O atoms (24*d* and 4*b*) and one partially occupied O atom (8*c*) are present. It needs to be pointed out that in the structure of HT ZrW_2O_8, the coordinates of the oxygen atom at the 8*c* Wyckoff position was fixed at 0.5055 as the refined value was fluctuating at 0.5 ± 0.055. Thus, it may be concluded that the structure of $ZrV_{1.50}Mo_{0.50}O_{7.25}$ is very closely related to that of HT ZrW_2O_8.

The polyhedral representation of the crystal structure is presented in Figure 2. There are two kinds of V1/Mo1−O distances in $[(V/Mo)O_4]^{3-}$ tetrahedra making the tetrahedra distorted. The bond distances are 1.7302(10) Å and 1.694(2) Å for the longer V1/Mo1−O1 and three shorter V1/Mo1−O2

dx.doi.org/10.1021/ic201224g |*Inorg. Chem.* 2011, 50, 8774–8781

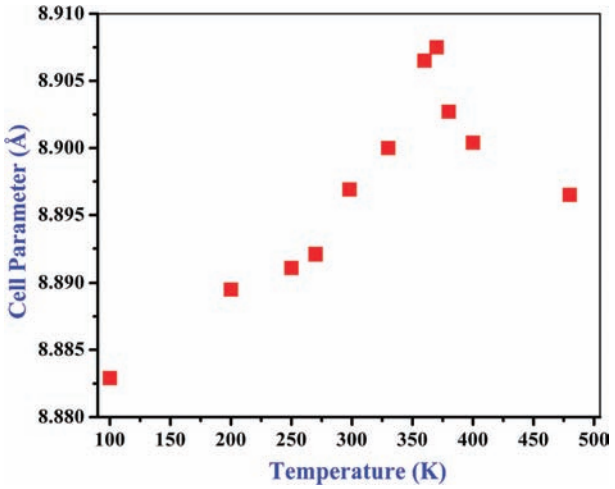

Figure 3. Graphical representation of variation of cell parameter with temperature of the single crystal.

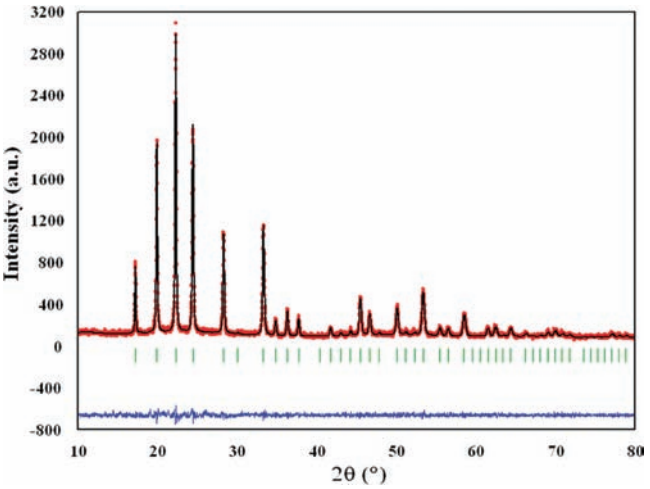

Figure 5. Observed, calculated, and difference powder XRD pattern for $ZrV_{2-x}Mo_xV_2O_{7+\delta}$ for $x = 0.8$.

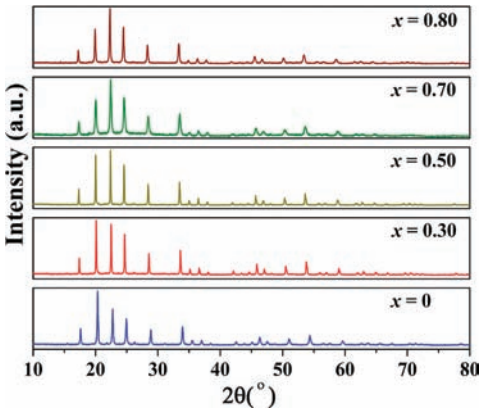

Figure 4. Powder XRD profiles of various members of the solid solution $ZrV_{2-x}Mo_xO_{7+\delta}$ $(0 \le x \le 0.8)$.

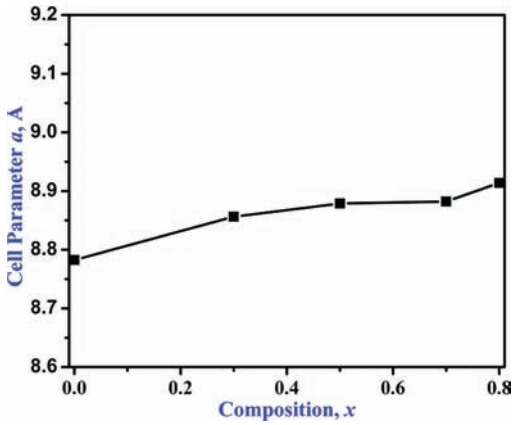

Figure 6. Variations in cell parameter with compositions.

distances in the tetrahedra, respectively. The O1 acts as the bridging atom between two $[(V/Mo)O_4]^{3-}$ tetrahedra to create a pyro(vanadate/molybdate) moiety. Similarly, there are two kinds of Mo2−O distances; the longer (Mo2−O1A = 1.69(3) Å) and three shorter (Mo2−O2 = 1.629(2) Å) distances. Zr atoms form perfect octahedra with six equal Zr−O2 distances with bond lengths equal to 2.059(2) Å.

Thermal Expansion Studies. As the parent compound ZrV_2O_7 displays negative thermal expansion above 102 °C, thermal expansion studies were carried out for the Mo substituted ZrV_2O_7 single crystal from 100 to 480 K on the same single crystal. The cell parameter increased with an increase in temperature from 100 to 370 K from 8.8829(2) to 8.9075(2) Å. At this temperature, the negative expansion region begins with the cell parameter decreasing steadily from 8.9075(2) to 8.8965(3) Å with the temperature changing from 370 to 480 K. Table 5 shows the cell parameter values as a function of temperature in the range of 100 to 480 K. The phase transition temperature is 370 K as realized from Figure 3. It must be highlighted that in ZrV_2O_7, the negative thermal expansion begins at 375 K. The linear thermal expansion coefficient α_a calculated in the temperature range 370 to 480 K is found to be -11.226×10^{-6} K^{-1}. It is of interest to note that the thermal expansion coefficient[36] of ZrV_2O_7 is -7.1×10^{-6} K^{-1} in the temperature range of 400 to 500 K. This indicates that the negative thermal expansion of Mo substituted ZrV_2O_7 is approximately 1.6 times that of ZrV_2O_7.

Laboratory Powder XRD Data. Laboratory powder XRD confirmed the phase purity of the various compositions in the series $ZrV_{2-x}Mo_xV_2O_{7+\delta}$ $(0 \le x \le 0.8)$, synthesized by the combustion synthesis method. Figure 4 shows the powder XRD profiles of various members of the solid solution. For all the compositions, profile refinements on powder X-ray data were carried out using JANA2000 using the structural model obtained from the single crystal data of the Mo doped ZrV_2O_7. The observed, calculated, and difference profiles for the highest limit of the solid solution of the composition $x = 0.8$ are presented in Figure 5. The cell parameter "*a*" increases with increase in Mo substitution in the solid solution $ZrV_{2-x}Mo_xV_2O_{7+\delta}$ $(0 \le x \le 0.8)$ as shown in Figure 6.

To establish the nature of the compositions above the limits of the solid solution, we have synthesized various compositions above $x = 0.8$ by combustion synthesis. Compositions above the value of $x = 0.8$ present a mixture of two phases. One phase is the ZrV_2O_7 related phase and the other phase is the α-$ZrMo_2O_8$ (trigonal polymorph of $ZrMo_2O_8$). Supporting Information, Figure S2 presents the profile fitting for the composition $x = 1.0$, where the powder pattern is a mixture of two phases.

dx.doi.org/10.1021/ic201224g |*Inorg. Chem.* 2011, 50, 8774–8781

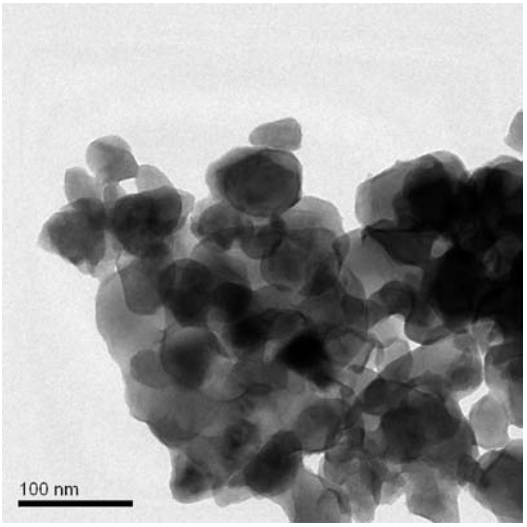

Figure 7. TEM image showing the particle size of the combustion synthesized ZrV_2O_7.

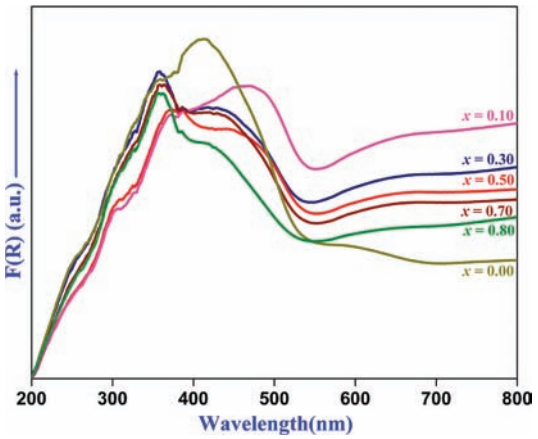

Figure 8. Solid state UV−vis diffuse reflectance spectra for various compositions of the solid solution.

Morphology, Compositional Analysis, and UV−vis Spectra. As $ZrV_{2-x}Mo_xV_2O_{7+\delta}$ ($0 \le x \le 0.8$) has been synthesized for the first time by combustion synthesis, further characterization of the samples has been carried out by obtaining TEM images (Figure 7) and performing Energy-dispersive X-ray (EDX) analysis (on the compositions 0, 0.3, and 0.7 of $ZrV_{2-x}Mo_xV_2O_{7+\delta}$), which are shown in Supporting Information, Figure S3. The TEM images show a particle size of 30 to 40 nm for the combustion synthesized samples. They also confirm the nanosize of the samples. EDX analysis confirmed the presence of Zr, O, V and Zr, O, V, Mo only for the pure and Mo doped samples, respectively. The formula derived from the EDX analysis was commensurate with the compositions. Room temperature UV−vis spectra were collected in the diffuse reflectance mode for various compositions in the series $ZrV_{2-x}Mo_xV_2O_{7+\delta}$ ($0 \le x \le 0.8$). The diffuse reflectance spectra were converted to absorbance like spectra using the Kubelka−Munk function (Figure 8). All the spectra show a broad absorption band starting from 800 to 200 nm. The experimental band gaps for these compositions were calculated to be 1.8 to 2.0 eV.

Photocatalysis. Photocatalytic degradation of both cationic dyes (MB and RB) and anionic dyes (anthraquinonic, diazo and monoazo) were studied. For the degradation experiments, the lamp position in the photochemical reactor was adjusted such that no degradation was observed either in the absence of UV light or catalyst alone. Photocatalytic degradation of the dyes MB, OG, RBBR, RB, MO, AO6, and AO7 in presence of $ZrV_{2-x}Mo_xV_2O_{7+\delta}$ catalysts was investigated in this work. XRD patterns taken before and after the reaction indicate no structural change of the catalyst ZrV_2O_7 (Supporting Information, Figure S4).

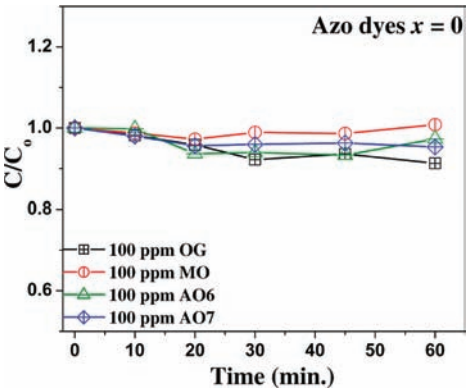

Figure 9. UV degradation profiles of azo dyes by ZrV_2O_7.

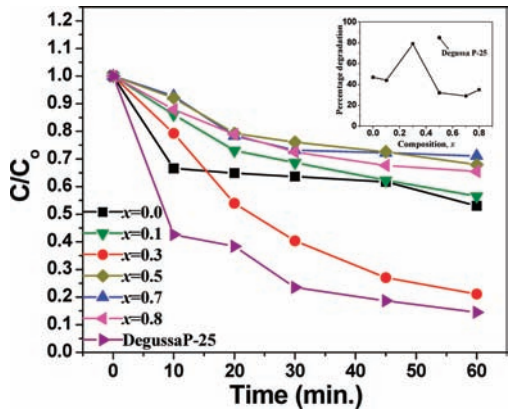

Figure 10. UV degradation profiles of RB with initial concentration of 20 ppm by various compositions of the solid solution.

As seen from Figure 9, the catalyst did not degrade azo dyes like OG, MO, AO6, and AO7. Figure 10 shows the degradation of RB in the presence of the $ZrV_{2-x}Mo_xV_2O_{7+\delta}$ series with $x = 0$, 0.1, 0.3, 0.5, 0.7, and 0.8 compositions. To compare the activity of these compounds with standard material, experiments were also conducted with Degussa P-25 TiO_2. These oxides significantly degrade RB for $x = 0.3$ composition, but the degradation is lower at lower Mo content ($x = 0$, 0.1) and also at higher Mo content ($x = 0.5$, 0.7, 0.8). This is clearly shown in the plot (inset of Figure 10) of percentage degradation as a function of Mo composition. It is also observed that the activity of $ZrV_{2-x}Mo_xV_2O_{7+\delta}$ with $x = 0.3$ is very similar to the activity of Degussa P-25 TiO_2, as observed from Figure 10.

To confirm this trend, the degradation of MB and RBBR dyes in the presence of $ZrV_{2-x}Mo_xV_2O_{7+\delta}$ series with $x = 0$, 0.3, and 0.7 compositions were carried out. It can be observed from Figure 11 that catalysts with $x = 0$, 0.3, and 0.7 do not degrade the MB dye significantly. These observations are consistent with the observations reported in our previous work on open framework

dx.doi.org/10.1021/ic201224g |*Inorg. Chem.* 2011, 50, 8774–8781

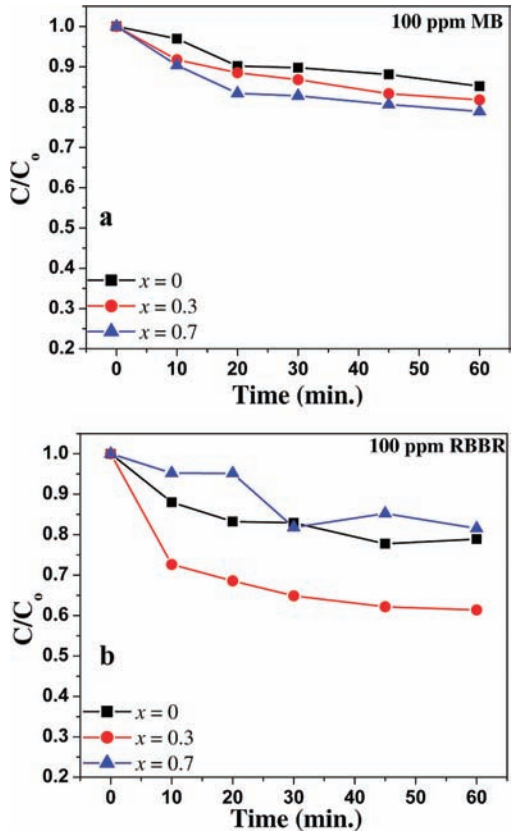

Figure 11. UV degradation of (a) MB and (b) RBBR by $x = 0$, 0.3, and 0.7 samples.

$ZrMo_2O_8$.[24,25] Similarly the RBBR dye degradation increases for $x = 0.3$ compared to $x = 0$, but again it is suppressed for $x = 0.7$ composition. Thus, the substitution of Mo in ZrV_2O_7 increases the photocatalytic activity for $x = 0.3$ but decreases on further substitution of Mo in ZrV_2O_7.

This indicates that the compounds synthesized in this study have the maximum activity when $x = 0.3$, but all compounds do not degrade the azo dyes. The specificity of these compounds to degrade non-azo dyes could be due to the inability of these catalysts to break the N−C bond adjacent to the azo moiety which is the crucial step in the degradation of azo dyes as suggested in other studies.[37] Specificity of compounds to the degradation of specific dyes and compounds has been reported earlier[14,15] This is the first study on the photocatalytic activity of ZrV_2O_7 with and without Mo doping. However, the effect of Mo doping on the photocatalytic activity of other compounds has been investigated. In this study, an optimum concentration of Mo was observed for best photocatalytic activity. Similar results have been observed for Mo doped TiO_2 wherein an optimum Mo concentration leads to higher photocatalytic activity.[38] This optimal concentration was attributed to the maximum width in the space charge region wherein charge carriers are effectively separated. In our previous study, Mo was substituted in place of V in $CeVO_4$. In that case, the conduction band consisted of V 3d and Mo 4d, and the higher photocatalytic activity of Mo substituted $CeVO_4$ was attributed to the presence of regular VO_4 and MoO_4 tetrahedra, which is beneficial for the charge transfer.[14] Other groups have investigated the photocatalytic activity of Mo substituted $BiVO_4$. The higher photocatalytic activity was attributed as due to increase of the surface acidity because of Mo substitution.[39] In our study, we have also observed higher activity of Mo substituted ZrV_2O_7 for the degradation of cationic dyes such as MB and RB.

CONCLUSIONS

A new solid solution $ZrV_{2-x}Mo_xO_{7+\delta}$ ($0 \le x \le 0.8$) has been identified in the phase diagram of $ZrO_2-V_2O_5-MoO_3$. These compounds were synthesized via the solution combustion method for the first time. The single crystals of the molybdovanadate were grown by the melt-cool technique. The single crystal structure revealed the structural similarities between the Mo substituted ZrV_2O_7 and HT ZrW_2O_8 crystal structure. The variable temperature single crystal XRD indicated negative thermal expansion above 370 K for the Mo substituted ZrV_2O_7 single crystal. The photocatalytic activity of the compound has been investigated for the degradation of various dyes, and this showed the specificity of the compounds toward the degradation of non-azoic dyes.

ASSOCIATED CONTENT

Supporting Information. CIF: The CIFs for the single crystal XRD for room temperature, 200 and 400 K; Schematic diagram of all the dyes studied. (Table S1); Video micrograph of Single-crystal of Mo doped ZrV_2O_7 (Figure S1); Full pattern matching of the powder XRD pattern of the composition $x = 1.0$ for $ZrV_{2-x}Mo_xO_{7+\delta}$ (Figure S2); EDX images for compositions $x = 0$, 0.3, and 0.7 (Figure S3); Powder XRD pattern of ZrV_2O_7 before and after degradation of Methylene Blue (Figure S4). This material is available free of charge via the Internet at http://pubs.acs.org.

AUTHOR INFORMATION

Corresponding Author

*E-mail: ssctng@sscu.iisc.ernet.in. Phone: +91-80-22932796. Fax: +91-80-23601310.

ACKNOWLEDGMENT

P.P.S. thanks the Indian Institute of Science for a senior research fellowship. We acknowledge funding (SR/S1/IC-13/2008) from DST-India. We thank DST-FIST (level II) for funding the Oxford diffraction X-ray facility.

REFERENCES

(1) Peyronel, G. *Gazz. Chim. Ital.* **1942**, *72*, 77.
(2) Craig, D. F.; Hummel, F. A. *J. Am. Ceram. Soc.* **1972**, *55*, 532.
(3) Korthuis, V.; Khosrovani, N.; Sleight, A. W.; Roberts, N.; Dupree, R.; Warren, W. W. *Chem. Mater.* **1995**, *7*, 412.
(4) Evans, J. S. O.; Hanson, J. C.; Sleight, A. W. *Acta Crystallogr., Sect. B: Struct. Sci.* **1998**, *54*, 705.
(5) Khosrovani, K.; Sleight, A. W.; Vogt, T. *J. Solid State Chem.* **1997**, *132*, 355.
(6) Withers, R. L.; Evans, J. S. O.; Hanson, J.; Sleight, A. W. *J. Solid State Chem.* **1998**, *137*, 161.
(7) Carlson, S.; Andersen, A. M. K. *J. Appl. Crystallogr.* **2001**, *34*, 7.
(8) Hemamala, U. L. C.; El-Ghussein, F.; Muthu, D. V. S.; Andersen, A. M. K.; Carlson, S.; Ouyang, L.; Kruger, M. B. *Solid State Commun.* **2007**, *141*, 680.
(9) Buchanan, R. C.; Wolter, G. W. *J. Electrochem. Soc.* **1983**, *130*, 1905.

(10) Lahiri, S.; Roy, K.; Bhattacharya, S.; Maji, S.; Basu, S. *Appl. Radiat. Isot.* **2005**, *63*, 293.
(11) Hisashige, T.; Yamaguchi, T.; Tsuji, T.; Yamamura, Y. *J. Ceram. Soc. Jpn.* **2006**, *114*, 607.
(12) Duc, F.; Gonthier, S.; Brunelli, M.; Trombe, J. C. *J. Solid State Chem.* **2006**, *179*, 3591.
(13) Zema, M.; Ghigna, P.; Tarantino, S. C. *J. Solid State Chem.* **2007**, *180*, 577.
(14) Mahapatra, S.; Madras, G.; Row, T. N. G. *J. Phys. Chem. C* **2007**, *111*, 6505.
(15) Hegde, M. S.; Madras, G.; Patil, K. C. *Acc. Chem. Res.* **2009**, *42*, 704.
(16) Patil, K. C.; Aruna, S. T.; Mimani, T. *Curr. Opin. Solid State Mater. Sci.* **2002**, *6*, 507.
(17) Galindo, C.; Jacques, P.; Kalt, A. *Chemosphere* **2001**, *45*, 997.
(18) Fujishima, A.; Zhang, X. T. *C. R. Chim.* **2006**, *9*, 750.
(19) Kim, H. G.; Becker, O. S.; Jang, J. S.; Ji, S. M.; Borse, P. H.; Lee, J. S. *J. Solid State Chem.* **2006**, *179*, 1214.
(20) Pieck, C. L.; del Val, S.; Granados, M. L.; Banares, M. A.; Fierro, J. L. G. *Langmuir* **2002**, *18*, 2642.
(21) Pieck, C. L.; Banares, M. A.; Fierro, J. L. G. *J. Catal.* **2004**, *224*, 1.
(22) Sasikala, R.; Sudarsan, V.; Sakuntala, T.; Jagannath; Sudakar, C.; Naik, R.; Bharadwaj, S. R. *Appl. Catal., A* **2008**, *350*, 252.
(23) Ge, J. Z.; Xue, M. W.; Sun, Q.; Auroux, A.; Shen, J. Y. *J. Mol. Catal A: Chem.* **2007**, *278*, 209.
(24) Sahoo, P. P.; Sumithra, S.; Madras, G.; Row, T. N. G. *J. Phys. Chem. C* **2009**, *113*, 10661.
(25) Sahoo, P. P.; Sumithra, S.; Madras, G.; Row, T. N. G. *Bull. Mater. Sci.* **2009**, *32*, 337.
(26) Patil, K. C.; Aruna, S. T.; Ekambaram, S. *Curr. Opin. Solid State Mater. Sci.* **1997**, *2*, 158.
(27) Dusek, M.; Petricek, V.; Wunschel, M.; Dinnebier, R. E.; van Smaalen, S. *J. Appl. Crystallogr.* **2001**, *34*, 398.
(28) *CrysAlis CCD and CrysAlis RED*, 1.171.33.31; Oxford Diffraction Ltd.: Abingdon, Oxfordshire, England, 2009.
(29) Sheldrick, G. M. *Acta Crystallogr., Sect. A* **2008**, *64*, 112.
(30) Farrugia, L. J. *J. Appl. Crystallogr.* **1999**, *32*, 837.
(31) Brandenburg, K. *DIAMOND*, version. 3.2e; Crystal Impact GbR: Bonn, Germany, 1999.
(32) Wang, X. D.; Heier, K. R.; Stern, C. L.; Poeppelmeier, K. R. *Inorg. Chem.* **1998**, *37*, 6921.
(33) Mary, T. A.; Evans, J. S. O.; Vogt, T.; Sleight, A. W. *Science* **1996**, *272*, 90.
(34) Lind, C.; Wilkinson, A. P.; Hu, Z. B.; Short, S.; Jorgensen, J. D. *Chem. Mater.* **1998**, *10*, 2335.
(35) Evans, J. S. O.; Mary, T. A.; Vogt, T.; Subramanian, M. A.; Sleight, A. W. *Chem. Mater.* **1996**, *8*, 2809.
(36) Evans, J. S. O. *J. Chem. Soc., Dalton Trans.* **1999**, 3317.
(37) Vinu, R.; Akki, S. U.; Madras, G. *J. Hazard. Mater.* **2010**, *176*, 765.
(38) Devi, L. G.; Murthy, B. N.; Kumar, S. G. *J. Mol. Catal. A: Chem.* **2009**, *308*, 174.
(39) Yao, W.; Iwai, H.; Ye, J. *Dalton Trans.* **2008**, 1426.